Quantum Chemical Molecular Dynamics Model Study of Fullerene Formation from Open-Ended Carbon Nanotubes†

Guishan Zheng,‡ Stephan Irle,*,§ Marcus Elstner,||,⊥ and Keiji Morokuma*,‡,§

Department of Chemistry, Emory University, Atlanta, Georgia 30322, Cherry L. Emerson Center for Scientific Computation, Emory University, Atlanta, Georgia 30322, Deutsches Krebsforschungszentrum, Abteilung Molekulare Biophysik, Im Neuenheimer Feld 280, 69120 Heidelberg, Germany, and Universität Paderborn, Fachbereich Physik, 33095 Paderborn, Germany

Received: October 31, 2003; In Final Form: January 29, 2004

We present quantum chemical molecular dynamics (MD) simulations for a model formation process of fullerene molecules. Trajectories of up to 24-ps lengths were computed for (5,5), (7,3), (8,0), (9,0), (10,0), and (10,5) open-ended single-walled carbon nanotubes for a temperature range between 2000 and 4000 K at various tube lengths, using density functional based tight-binding (DFTB) molecular dynamics. DFTB was selected because geometries and energies obtained are found to qualitatively agree with B3LYP/6-31G(d) results at much smaller cost of computer time. Extremely fast cage formation was observed with simulation times as short as 3 ps, and most simulations at 3000 and 4000 K led to the formation of fullerene structures within less than 14-ps simulation times. Key structural features for the transformation of tubes to fullerenes are identified, such as the overwhelming presence of acetylenic "wobbling C_2 units", which form spontaneously in great abundance at the open ends of the tubes. A comparison of DFTB simulations is made with corresponding semiclassical reactive bond-order force field MD trajectory calculations, which exhibit much slower structural transformations without the "wobbling" C_2 units. We also compare DFTB energetics of optimized MD snapshot structures with B3LYP energies.

I. Introduction

In 1985, Kroto et al. discovered that the C_{60}^+ fullerene cation is an unusually stable species among the gas-phase carbon ions produced by laser vaporization of graphite.[1] After Krätschmer et al. found a method to synthesize macroscopic quantities of fullerenes,[2] experimental and theoretical research on fullerene chemistry has become one of the most active fields in today's nanochemistry. However, how such a highly symmetric hollow cage structure is formed under the chaotic high-temperature conditions of vaporized carbon remains an unsolved mystery and has been the topic of many discussions. Understanding the formation mechanism of fullerene molecules is a necessary prerequisite to optimize efficient fullerene generation techniques, which could stimulate the development of new fullerene-based materials.

Current fullerene synthesis methods are harsh and involve either vaporization of graphite by laser, electric arc discharge, plasma,[3] or combustion of acetylene, benzene, or toluene in hot, oxygen-rich diffusion flames under low pressure.[4−9] During these synthetic procedures, it has so far been impossible to detect important intermediate structures against a background of all different kinds of carbonaceous material. As a result, the proposed mechanisms are more or less guesswork, relying on the assumption of orderly growth along a certain reaction pathway from well-defined precursor species and intermediate structures. The most prominent ones are, in chronological order, the "nautilus model",[10,11] the "party line" mechanism,[12] the "pentagon road",[13−15] the "fullerene road",[16] the "ring-stacking" mechanism,[17] and the "ring fusion spiral zipper" mechanism.[18−20] Reviews[21,22] give an overview of these proposed reaction pathways.

In the past, numerous quantum chemical electronic structure calculations on hypothetical intermediates of these proposed fullerene formation mechanisms have been performed.[23−26] Moreover, Mishra et al. attempted to locate transition state structures connecting intermediate structures and describing entire pathways for the formation of C_{28} fullerene through their "ring-collapse" mechanism at the semiempirical AM1[27] level of theory, starting from small monocyclic carbon rings such as C_9 and C_{13}.[28] However, it is more than questionable whether an orderly growth process along a single or a few reaction pathways with well-defined transition states and intermediate structures is a realistic assumption under the high-temperature nonequilibrium conditions characteristic for fullerene formation. The large amount of kinetic energy available under the experimental conditions allows carbon clusters to climb upward on hills on the potential-energy surface rather than to cling to a specific minimum-energy reaction pathway. To this end, Monte Carlo simulations[29] and molecular dynamics (MD) studies have been carried out before, all of them using reactive empirical bond-order (REBO) Tersoff-type[30,31] interatomic carbon−carbon potentials developed originally for studying the vapor deposition of diamond.[32,33] Unlike traditional molecular mechanics force fields, the REBO potential allows for the formation and dissociation of covalent chemical bonds by determination of nearest neighbors and on-the-fly switching bond

† Part of the special issue "Fritz Schaefer Festschrift".

* Authors to whom correspondence may be addressed. E-mail: sirle@emory.edu (S.I.); morokuma@emory.edu (K.M.).

‡ Department of Chemistry, Emory University.

§ Cherry L. Emerson Center for Scientific Computation, Emory University.

|| Abteilung Molekulare Biophysik.

⊥ Universität Paderborn.

10.1021/jp0373090 CCC: $27.50
Published on Web 03/10/2004

functions. However, it has been criticized that the REBO potential is only successful in describing *intramolecular* interactions in carbon and hydrocarbon materials and that it lacks a mechanism for treating *intermolecular* interactions,[34] which is a severe flaw for the description of a hot mixture of small carbon fragments. Even more seriously, REBO-type molecular force fields including the one improved by Brenner in 2000[35] do not take into account π-conjugational effects since REBO was designed to only describe the formation and breaking of carbon−carbon σ-bonds. However, aromaticity and π-conjugational stabilization are important factors in fullerene chemistry, and therefore we felt compelled to carry out the first full quantum chemical MD (QM/MD) simulations in a model study on the formation of fullerenes from open-ended single-walled carbon nanotubes. We believe that, even though carbon nanotubes as initial structures are certainly a somewhat artificial choice for the study of fullerene formation, the knowledge of "major players" emerging from such QM/MD simulations will lead to a deeper understanding of structure transformation mechanisms in carbon nanochemistry. Because of its computational feasibility and relatively good agreement with B3LYP, we selected the density functional tight binding (DFTB) quantum chemical potential[36,37] for these MD simulations.

We have published a short communication of the DFTB trajectories of open-ended single-walled carbon nanotubes[38] and pointed out the importance of acetylenic "wobbling C_2 units" consisting of sp-hybridized carbons for the creation of pentagons. The present paper is a follow-up of this communication and consists of five results and discussion sections. First, DFTB relative energies for different isomers of C_{28} are systematically compared with those of the B3LYP/6-31G(d) hybrid density-functional level of theory. Second, we review in detail results of DFTB MD simulations on (5,5), (7,3), (8,0), (9,0), (10,0), and (10,5) open-ended single-walled carbon nanotubes of different tube lengths that are subjected to a temperature between 1000 and 4000 K for as long as 24 ps. Common features of these simulations are described in detail, and important key steps on the pathway to fullerene formation are identified. Third, to access what kind of structures and potential energies are actually visited during the trajectories, 10 snapshot structures at 1.2-ps intervals are taken and compared with the structures optimized from these snapshot points. At these optimized points, the DFTB relative energies were also compared with single point B3LYP/6-31G(d) energies, to assess the reliability of the DFTB energies. Fourth, the strengths of rim CC bonds in (5,5) and (9,0) open-ended nanotubes were computed at the DFTB level and compared with the trends of the initial bond-breaking activities during the trajectories. Finally, REBO MD simulations on (5,5) and (7,3) open-ended single-walled carbon nanotubes are presented, and the difference with DFTB MD is discussed.

II. Computational Details

The density-functional tight binding (DFTB) method is the central method adopted in the present studies. All DFTB calculations were carried out with the DFTB program package developed by Frauenheim, Seifert, and Elstner.[36,37,39] DFTB is an approximate density functional theory method based on the tight binding approach and utilizes an optimized minimal LCAO Slater-type all-valence basis set in combination with a two-center approximation for Hamiltonian matrix elements. Although calculations were performed mainly for the closed-shell state, when energy differences between occupied and vacant orbitals are smaller than 10^{-4} Hartree for a given geometry, these orbitals are considered to be degenerate, and an open shell occupancy is automatically adopted. While the total energy is not affected by the choice of occupancy of degenerate orbitals, the energy gradient depends on this choice. The DFTB code used the conjugate gradient method for geometry optimization. Direct DFTB trajectories were run by calculating analytical energy gradient on the fly with a velocity Verlet integrator, using 1.209 fs (50 atomic units) as the time steps Δt. This time step, larger than what is often used, is adopted since the system contains no light hydrogen atoms. By use of this time step, energy is conserved typically within a range of about ± 7 kcal/mol, which is sufficiently accurate for the purposes of this study. Temperature was kept constant by scaling of atomic velocities in two ways. For one, scaling was regularly performed after 12 fs, and additionally random scaling was performed with a probability of 10%, thereby an overall probability of scaling velocities was 20% for the entire length of the simulations. (In the case of a (5,5) tube with 7.5-Å length at 3000 K, we tested scaling of temperature at a lower rate (5%) and actually observed faster closing of both ends, indicating that a scaling probability of 20% does not artificially speed up the dynamics simulation.) Initial velocities were assigned randomly. All calculations were carried out using a 30-Å cubic periodic cell. The temperatures applied in our simulations ranged between 1000 and 5000 K. Because the cost of on-the-fly quantum chemical calculations is substantially higher than molecular mechanics force field calculations, we ran only one trajectory for each type and length of nanotube at a given temperature.

The B3LYP hybrid density functional method was used in combination with the 6-31G(d) basis set as benchmark method. The Gaussian 01 development version[40] was used for these calculations.

Two select trajectories were also run using the original reactive empirical bond-order (REBO) force field, the so-called Brenner potential,[32,32] with the REBO code available at the following website: http://www.mse.ncsu.edu/CompMatSci/. The same step size of 1.209 fs and the Berendsen thermostat were used here to keep the temperature constant. MacMolPlt[41] was used for graphics visualization of all trajectories.

III. Results and Discussion

A. Comparison of DFTB Relative Energies of Isomeric C_{28} Structures with B3LYP/6-31G(d). Because of the limitations in computational resources, semiempirical methods are a good compromise between accuracy and speed in quantum chemical calculations for large molecules. DFTB has been successfully used in the past to explain relative stabilities of fullerene isomers and aggregates.[42−46] It is well-known that neutral carbon clusters adapt different configurations upon cluster growth. C_n clusters with $n \leq 5$ prefer linear cumulene-type structures, and in the intermediate regime of $6 \leq n < 18$, monocyclic isomers are preferred before fullerenoid structures become the most stable species for $n \geq 18$.[25,42] In contrast to the semiempirical AM1[27] and PM3[47] methods, DFTB is capable of reproducing these crucial configuration preferences for carbon clusters and more in line with the full DFT calculations such as B3LYP/6-31G(d).

Table 1 shows the relative energies of 11 singlet isomers of C_{28} calculated with benchmark B3LYP/6-31G (taken from ref 26), B3LYP/6-31G(d), and DFTB methods at respectively optimized geometries and with the B3LYP/6-31G(d) method at DFTB-optimized geometries. Linear regression analysis using B3LYP/6-31G(d) energetics as reference indicates very good correlation of DFTB with a correlation coefficient R^2 of 0.7571. In fact, B3LYP/6-31G(d) single point energies for DFTB optimized geometries show a correlation close to 1 with

TABLE 1: Relative Energies (in eV) of 11 Different Isomeric Singlet Structures of C_{28} Calculated with B3LYP/6-31G, B3LYP/6-31G(d), and DFTB

structure[a]	B3LYP/6-31G[b]	B3LYP/-6-31G(d)	DFTB	B3LYP/6-31G-(d)//DFTB
buckyD2	0.00	0.00	0.00	0.00
ring	0.76	3.32	8.10	3.43
c24−6	1.99	3.17	3.56	3.66
2+2r14	2.90	5.08	9.66	5.22
2+2r16	3.87	6.01	10.25	6.13
c20−6o	4.34	5.41	5.52	5.96
c20−6m	4.48	5.57	5.62	6.09
2+4	4.63	7.97	10.28	8.52
central7	4.84	5.86	6.07	6.47
8+8	4.98	7.43	9.43	7.41
4+4	5.59	9.91	14.27	10.20
R^2 [c]	0.8339		7571	9925

[a] Structures are illustrated below, with the labels taken from ref 26. [b] Taken from ref 26. [c] Squared correlation coefficients R^2 in the linear regression analysis with B3LYP/6-31G(d) energies.

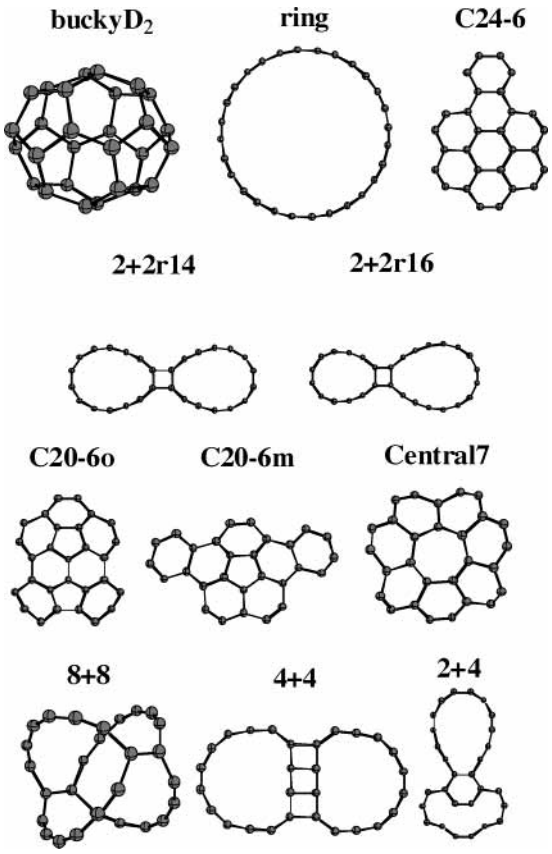

$R^2 = 0.9925$. As opposed to AM1, DFTB predicts the most stable and the least stable C_{28} isomers consistent with the B3LYP calculations.[48,49] The B3LYP/6-31G(d) single-point energies at the SCC-DFTB-optimized geometries correlate well with the B3LYP-optimized energies with $R^2 = 0.99$, indicating that the DFTB-optimized geometries are very reliable. From the above comparisons, we concluded that DFTB is acceptable in the description of isomers of C_{28} fullerene and decided to use DFTB as the semiempirical MO method of our choice for direct quantum chemical molecular dynamics (QM/MD) simulations.

B. High-Temperature DFTB Molecular Dynamics Trajectories. In our previous communication, we already described in detail trajectories at 3000 K for 7.5-Å (5,5) armchair and 7.5-Å (9,0) zigzag tube conversion to fullerenes and discussed common features displayed in similar trajectories. Here, we discuss all computed DFTB high-temperature molecular dynamics trajectories and focus on their energetics and differences for different temperatures and tube parameters. Additionally, trajectories for three nanotubes of 20-Å lengths with different chirality indices will be discussed in greater detail. Table 2 presents an overview of 52 computed trajectories of open-ended nanotubes at various temperatures. (Select trajectories can be found online on the Internet at http://euch4m.chem.emory.edu/nano/. All trajectories are available from the authors upon request.) Somewhat arbitrarily we consider a tube "closed" when the largest macrocyclic ring remaining in the opening does not contain more than 8 carbon atoms and mark first and second closing times by t_1 and t_2 if closure occurs. In total, we ran 52 trajectories between 1000 and 5000 K. At low temperatures around 1000 K, we found that the nanotubes are nonreactive, while all tubes simulated at 5000 K were destroyed and fell quickly apart, producing long entangled carbon chains within 5 ps. Most systems were therefore investigated at 2000, 2500, 3000, 3500, and 4000 K. Beside temperature, we chose to vary three tube parameters, namely, chirality, diameter, and lengths. In detail, the following models for open-ended carbon nanotubes were investigated: (a) Chirality: three different chiral types of (n,m) nanotubes were chosen that have about the same diameter d. ($d = (3/\pi)^{1/2}a((n^2 + nm + m^2))^{1/2}$, a being the C−C bond distance assumed as 1.40 Å.) They are the armchair (5,5), $d =$ 6.68 Å, chiral (7,3), $d = 6.86$ Å, and zigzag (9,0), $d = 6.95$ Å configurations. (b) Diameter: an (8,0) zigzag tube with a smaller diameter of $d = 6.17$ Å, a (10,0) armchair tube with a larger diameter of $d = 7.72$ Å, and a much larger chiral (10,5) nanotube with a diameter of $d = 10.21$ Å. (c) Length: three different tube lengths, 7.5, 10, and 20 Å, were used for most species. An important finding is that the diameters of the (10,5) and (10,0) nanotubes appear to be too large to allow the tube openings to be closed within 12 ps.

General Features of Trajectories. Because only a relatively small number of simulations have been performed, we do not claim statistical significance of the findings presented here. However, important dynamic ingredients common to all trajectories can be identified and discussed. The possibly most outstanding finding is that in most trajectories at 3000 and 4000 K at least one end of the tube is closed, forming a closed-cage structure within a short simulation time of 14 ps. As can be seen from Table 2, most QM/MD simulations maintained target temperatures on the average within 50 K with a slight tendency toward lower temperatures. Therefore, average temperature $\langle T \rangle$ and kinetic energy related to $\langle T \rangle$ by $\langle E_{kin} \rangle = {}^1/_2 k \langle T \rangle$ remain relatively constant. In this table, average relative potential energies per carbon atom $\langle V \rangle / n$ are given relative to one-half of the energy of a C_2 molecule. Since on the average temperature remains constant, $\langle V \rangle / n$ represents the profile of the total system energy during the simulation. An example of E_{kin} and V fluctuation and its average over 100 time steps is shown in Figure 1 for a 20-Å (9,0) nanotube at 3000 K. The potential energy per atom is fluctuating by as much as 4 kcal/mol. Common to all trajectories is a steep rise in $\langle V \rangle / n$ at the very beginning of the simulations, reflecting large geometrical distortions due to the abrupt exposure to high temperatures. As characteristic features in the energy profile of Figure 1, drops in $\langle V \rangle / n$ of about 2 kcal/mol can be seen when the open ends are closed at $t_1 = 11.69$ ps and $t_2 = 14.22$ ps. The trend toward lowering of potential energies when open tube ends are closed and dangling bonds become fully saturated is observable throughout the presented trajectories. Regarding $\langle V \rangle / n$ for same systems at various temperatures, it is certainly not surprising

TABLE 2: Summary of All the DFTB Trajectories of Nanotubes of Different Types and Lengths at Different Temperatures[a]

type (n,m)	length (Å)	no. carbon atoms, n	T (K)	$\langle T\rangle$ (K)	$\langle V\rangle/n$ (kcal/mol)	run time (ps)	t_1 (ps)	t_2 (ps)	no. lost $C_1\|C_2\|C_3$ units	no. final 4/5/6/7 rings
(5,5)	7.5	70	2000	2007	−66.8	11.89			0|0|0	1/4/21/1
			2500	2502	−64.6	11.89	7.47		0|0|0	0/9/20/2
			3000	3005	−62.3	23.78	11.69	14.22	0|1|0	1/12/17/4
			3000	3141	−63.7	23.8	1.64	4.93	2|0|0	1/11/23/1
			3500	3502	−55.0	11.89	4.75		0|1|0	0/6/6/4
			4000	3970	−40.1	11.89	2.20		destroyed	0/0/0/0
	10	90	1000	1006	−75.7	11.89				0/0/35/0
			2000	2003	−69.7	23.78	11.61	13.49	0|0|0	2/10/31/1
			2500	2503	−68.4	23.78	4.99	22.13	0|1|0	1/12/27/2
			3000	3002	−64.4	11.89	6.60	10.55	0|0|0	1/11/34/1
			3500	3515	−63.1	11.89	2.38	6.57		0/13/32/1
			4000	3985	−44.2	11.89	3.77	5.44	2|4|2	1/14/30/2
			5000	4952	−20.3	11.89			destroyed	0/0/0/0
	20	170	2000	2011	−74.4	9.46			0|0|0	0/0/71/0
			3000	2988	−69.4	5.35			0|0|0	0/8/66/2
			4000	4005	−59.7	14.21	1.28	3.39	3|5|0	0/14/53/1
			5000	4970	−29.8	10.45			destroyed	0/0/0/0
(7,3)	7.5	70	2000	1991	−65.0	11.90			0|0|0	0/3/20/0
			3000	2997	−60.3	11.90	7.73	11.84	0|0|0	1/12/16/3
			4000	3979	−39.9	11.90			destroyed	0/0/0/0
	10	98	1000	1014	−75.9	11.89			0|0|0	0/0/39/0
			2000	1997	−70.4	11.89			0|0|0	1/6/35/1
			2500	2507	−67.5	11.89	7.83		0|1|0	1/8/31/3
			3000	3004	−64.8	11.89	7.62	11.01	0|1|0	0/14/33/0
			3500	3507	−61.0	11.89	3.66	10.67	0|2|0	0/10/29/2
			4000	4002	−62.8	11.89			destroyed	0/0/0/0
	20	182	2000	1998	−74.6	7.92			0|0|0	0/0/77/0
			2500	2497	−71.7	7.76	6.83		0|0|0	2/5/74/1
			3000	3000	−68.9	7.92	3.89	7.48	0|4|0	1/11/74/1
			3500	3497	−65.5	7.50	1.62		0|1|0	0/8/71/2
			4000	4006	−59.8	8.26	1.63	5.75	2|6|1	0/12/63/5
			5000	4964	−37.1	7.68			destroyed	0/0/0/0
(8,0)	10	96	2000	1998	−69.3	11.89			0|0|0	2/5/74/1
			3000	2997	−57.4	11.89	4.43		0|2|0	1/7/26/4
			4000	4008	−56.5	11.89	6.49		0|1|0	0/9/29/0
(9,0)	7.5	90	2000	1992	−68.5	11.89			0|0|0	0/1/34/1
			3000	3008	−62.0	11.90	10.50		0|0|0	0/11/23/2
			4000	4004	−46.7	11.90	6.37		destroyed	0/0/0/0
	10	108	2000	2030	−69.3	9.98			0|0|0	0/2/41/2
			3000	3001	−64.3	11.66	7.22		0|0|0	0/9/27/4
			4000	3989	−47.5	11.90			destroyed	0/0/0/0
	20	180	2000	2004	−74.9	7.99			0|0|0	0/2/77/2
			3000	2992	−67.9	15.86	12.89	13.88	0|1|0	0/10/74/0
			4000	4008	−60.6	10.14	5.59	10.29	2|4|0	0/12/57/2
(10,0)	10	120	2000	1997	−70.9	8.09			0|0|0	0/50/0/0
			3000	2996	−64.5	7.61			0|0|0	1/5/37/0
			4000	4005	−54.2	7.10			0|5|0	1/5/19/3
(10,5)	10	140	1000	1009	−77.1	11.89			0|0|0	0/0/55/0
			2000	1997	−70.8	11.89			0|0|0	0/0/54/0
			3000	3001	−67.0	11.89			0|0|0	0/14/43/3
			4000	3996	−45.4	11.89			destroyed	0/0/0/0
			5000	4962	−24.7	11.89			destroyed	0/0/0/0

[a] Key: T is the target temperature, $\langle T\rangle$ is the actual average temperature, $\langle V\rangle/n$ is the average potential energy per C atom relative to a half of C_2 energy, t_1 is the time of closing of the first end, and t_2 is that of the other end (no entry here means that no closing occurred within the given simulation time). The numbers of C_1, C_2, and C_3 fragments lost and the numbers of four-, five-, six-, and seven-membered rings at the end of trajectory are also given. The *italic* trajectory was carried out using a 5% velocity scaling rate.

that this quantity rises in energy as temperature is increased, allowing the system to sample more frequently high energy structures. A comparison of $\langle V\rangle/n$ across systems for same temperatures reveals a striking similarity between relative stabilization energies, independent of system size and type. $\langle V\rangle/n$ values range between −65.0 and −74.9 kcal/mol for 2000 K, between −60.3 and −69.4 for 3000 K, and between −40.1 and −62.8 kcal/mol for 4000 K, with a tendency to overall lower potential energies for trajectories where tubes close early.

Concerning carbon fragments eliminated from the cluster, we find a prevalent dominance of C_2 units over carbon atoms and C_3 with a ratio of about 40:11:3. C_2 units and other fragments are very often lost when the tube closes but can also detach when the connecting bond of, e.g., wobbling C_2 units becomes vibrationally excited. As can be seen from Table 2, more fragments detach at higher temperatures. Because periodic boundary conditions forced these fragments to stay in the vicinity of the cluster, several reattachments of previously eliminated fragments have been observed, and we anticipate that under experimental conditions with a constant flow of C_2 units such attachment steps will significantly contribute to cluster growth and isomerization. A previous QM/MD study found similar attachments of carbon fragments on open-ended tubes.[50]

In the following paragraphs, we will discuss three different

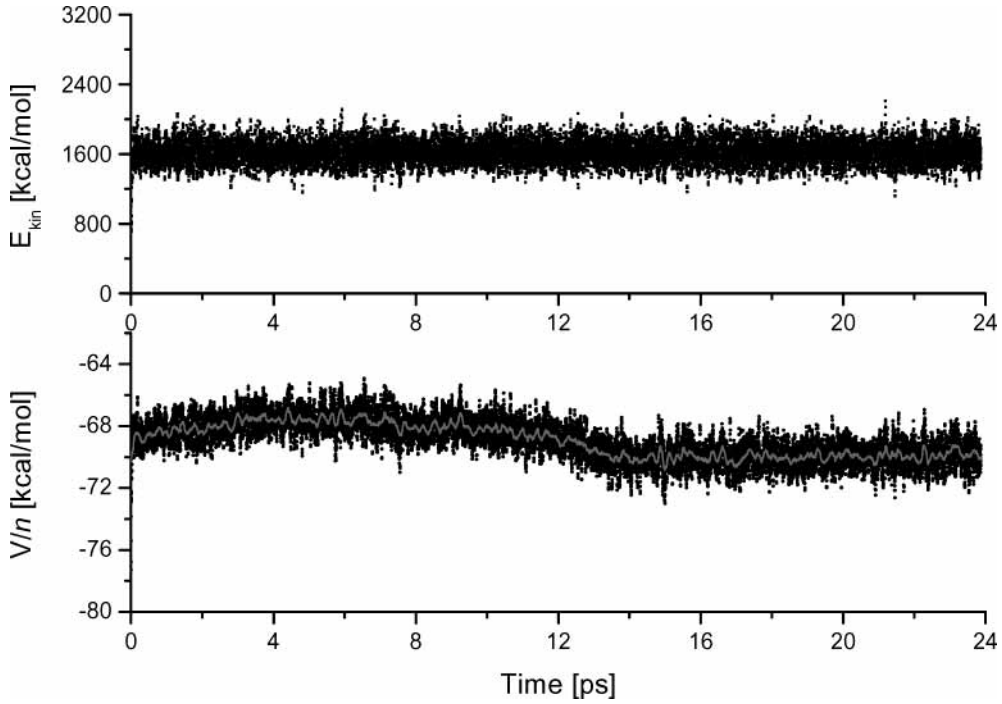

Figure 1. The potential-energy profile of the 20-Å (9,0) tube DFTB trajectory at 3000 K. Shown in this figure are kinetic energy and *V/n* potential energy.

nanotubes of 20-Å length, (5,5) at 4000 K and (7,3) and (9,0) at 3000 K. All three tubes close both ends in these trajectories within 14 ps but show very different dynamics behaviors at the beginning of the trajectories. Nevertheless, the number of pentagons formed at the end of these three trajectories is similar, namely, 14, 11, and 10 for (5,5), (7,3), and (9,0), respectively.

MD of a 20-Å (5,5) Tube at 4000 K. Figure 2 displays 17 snapshots for the simulation of a 20-Å armchair (5,5) tube at 4000 K, which starts with an intact tube possessing a perfect honeycomb hexagonal lattice at 0.00 ps. For brevity, we will distinguish the two ends of the tube by R for right and L for left. Because of the high temperature, this trajectory is very dynamic and contains features not often seen at temperatures around 3000 K. For instance, very early in the simulation, at 0.03 ps, it can be seen that a pentagon with an adjacent triangle is about to be created from a hexagon at R due to large vibrational amplitudes of the outer carbon atoms, while at the same time, a cisoid bond at the rear side of R also breaks leading to a wobbling C_2 unit attached to the rim. Other hexagons become strongly deformed along the entire tube, and several bonds become stretched beyond 1.8 Å but do not break. Immediately after the formation of an R triangle, one of its outer bonds breaks and a pentagon with one carbon atom attached to its top is formed at 0.07 ps. At the backside of R, the same type of structure is created by bond formation between the inner atom of the newly created wobbling C_2 unit and the unfilled valence of the adjacent carbon, which was originally connected to the outer C_2 atom. Such changes are observed very frequently for C_2 units and are a major source of pentagons in the cage-closing process. Large torsional deformations on both sides of the open-ended tube are visible in the 0.07-ps snapshot, but the L end remains completely intact while the R end undergoes further major transformation. At 0.11 ps, the rear R pentagon remains, the front pentagon is vibrationally strongly excited and undergoing restructuring, and a new pentagon is created again by catching the inner atom of a breakaway C_2 unit. As described before,[38] defect creation in nanotubes is a synergetically self-enhanced process; once a σ bond breaks, the π conjugation in this area is interrupted and the entire structural domain loses stability, leading to the formation of gradually more defects in the same area. The intact L end and the fractured R end of the 0.11-ps snapshot are good examples for this principle. While the R end undergoes further restructuring facilitated by large amplitude vibrations of defects and their conjunct hexagons, it is 0.53 ps for the L end to develop a wobbling C_2 unit by breaking a cisoid bond. The R end has meanwhile developed three wobbling C_2 units, and all pentagons have been back transformed to wildly moving hexagons. It is worth noting that the honeycomb structure of the inner portion of the tube remains intact and unchanged throughout these fast and pronounced modifications of the rims. At 0.62 ps, only 0.09 ps after the L end developed a long-lived wobbling C_2 unit, two more wobbling C_2 units are visible at L in the vicinity of the first one. The phenomenon of almost instantaneous creation of several wobbling C_2 units was dubbed "double wobbling" by us before.[38] These C_2 units are relatively vulnerable to becoming expelled by large amplitude vibrations, and at 0.74 ps, one of the R C_2 units can be seen to detach permanently from the tube, while at the L end another wildly vibrating C_2 unit is not leaving. However, the large number for C−C bonds longer than the threshold of 1.8 Å indicates that at 4000 K large amplitude vibrations are common and come close to destroying the entire tube as was found in all trajectories at 5000 K. At 0.92 ps, the R end loses a second wobbling C_2 unit and features a hexagon strongly bent inward at the tube opening, with two pentagons close by and at the opposite end of the opening. At 1.02 ps, a stable hexagon/pentagon combination has developed in the R opening with two adjacent pentagons. The bond between hexagon and pentagon in the opening is relatively weak and highly vibrationally excited, frequently allowing the carbon atoms of the "bridge" in the opening to approach the opposite side of the rim (see, e.g., 1.21 ps), leading to the complete closing of the opening at 1.28 ps. Meanwhile, the L end does not indicate signs of closing at all, featuring only one long-lived wobbling C_2 unit and no pentagons in this particular snapshot. It does, however, develop several pentagons over time

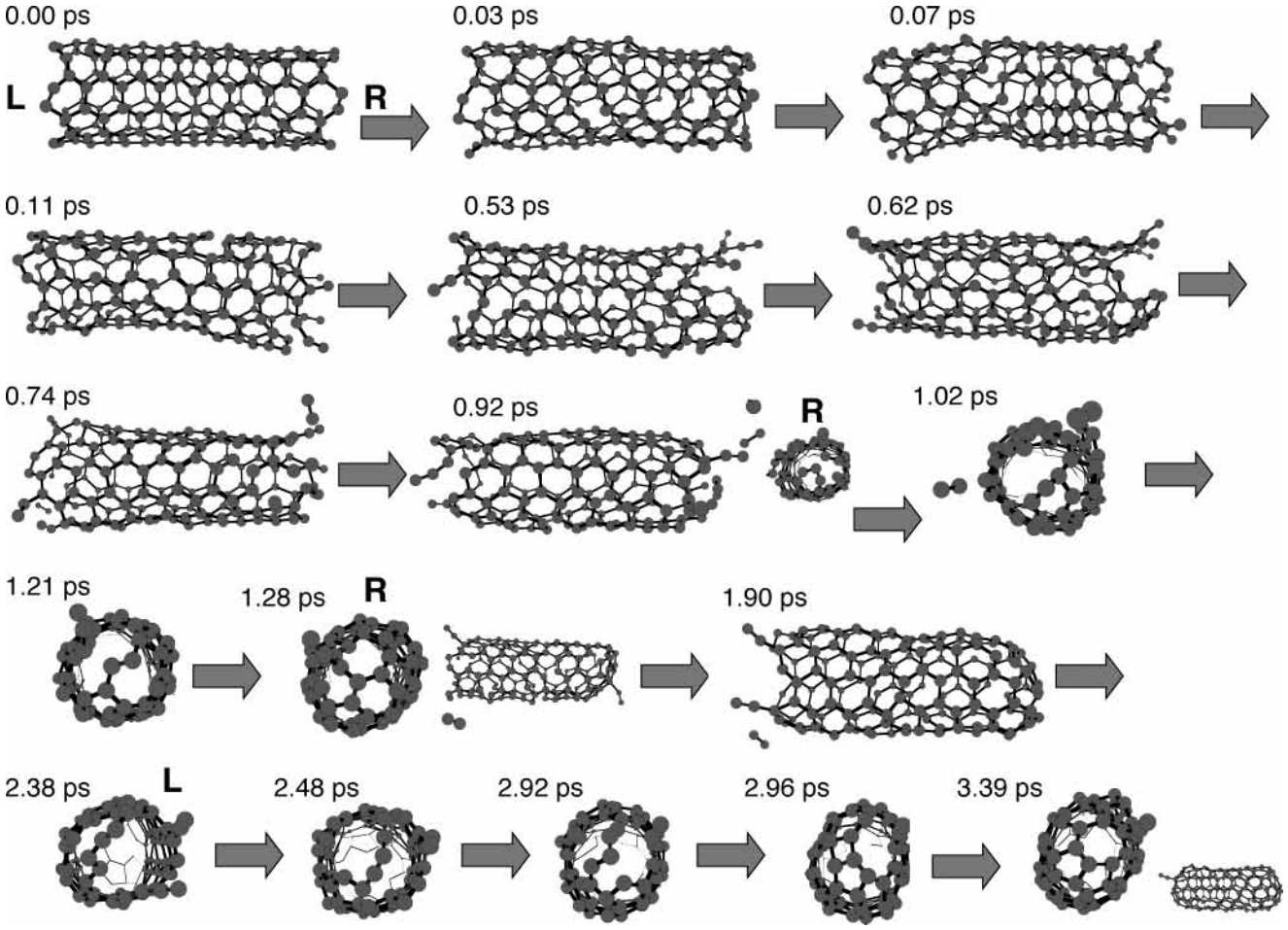

Figure 2. Snapshots of the DFTB trajectory of a 20-Å (5,5) tube at 4000 K.

by both of the aforementioned mechanisms and, at 1.90 ps, exhibits three wobbling C_2 units with one of them permanently leaving the tube. At that time, however, no pentagons have survived at the L end. The large amplitude motions finally lead to the creation of a long bridge from rim carbon chains in the center of the L opening at 2.38 ps, becoming part of a 15-atom macrocycle with two wobbling C_2 units at the opposite side of the rim. This bridge can make substantial movement within the opening as shown in the snapshot at 2.48 ps, allowing the wobbling C_2 units to connect if their conformation is suitable. At 2.92 ps, however, instead of the C_2 unit, an inward bent hexagon attacks the bridge from the opposite side of the rim, which leads to the gradual formation of two bridges in the opening at 2.96 ps. The highly strained four-membered rings contained in these bridges are subsequently involved in major, rapid reconstruction of this area and reactions with the rim atoms, leading at 3.39 ps to closure of the L opening as well. The result is a completely closed 20-Å (5,5) nanotube with 14 pentagons.

While low-temperature simulations of armchairs display smaller amplitude motions, wobbling C_2 formation can still be seen at 2000 K. C_n with $n > 2$ formation is rarely seen even at 4000 K. Common in all armchair simulations is the relative ease with which wobbling C_2 units can be formed from rim cisoid bonds. Pentagons are then very frequently created by its inner atom catching the original bond partner, leading to a single-carbon atom attached to the pentagon, which is always very reactive and tries to stabilize itself either by back transformation to a hexagon or by attacking neighbor units. Structural defects never grow larger than two layers from the rim, independent of temperature.

MD of a 20-Å (7,3) Tube at 3000 K. Figure 3 displays 13 snapshots, and as before, the left and right sides of the open ends are marked by L and R. The chiral nature of the tube can clearly be seen in the first snapshot at 0.00 ps. The edges of our model structures for chiral tubes are not homogeneously composed of either armchair- or zigzag-type structures but can be described as armchair "stairs" and have three "topmost" hexagons. All three of them at the R opening form almost simultaneously wobbling C_2 units after 0.10 ps by breaking cisoid bonds, while the configuration at L remains unchanged. This is another example that defects appear to be created in a self-enhanced manner and that unmodified carbon honeycomb lattices are very strong due to π conjugation. At 0.46 ps, one of the wobbling C_2 units catches the top atom of the "down-stairs" next-neighbored hexagon, thereby forming a clearly visible pentagon structure, while the L opening remains still in perfect shape with vibrationally excited but intact hexagons. At about the same time, another wobbling C_2 unit at R recombines to a hexagon, and only one wobbling C_2 unit remains at R. It has a longer lifetime and is still present after 0.97 ps, when simultaneously two cisoid bonds at L break along the same "staircase". Both ends feature multiple wobbling C_2 units from thereon, and a tendency toward creation of wobbling C_3 and C_4 units from the outer rim members of the same staircase can be seen frequently, e.g., at 2.10 ps. Here, the R end displays nicely how the wobbling C_4 units are created, while wobbling C_2, C_3, and C_4 units are also present at the same opening. The formation of longer wobbling C_n ($n > 2$) chains

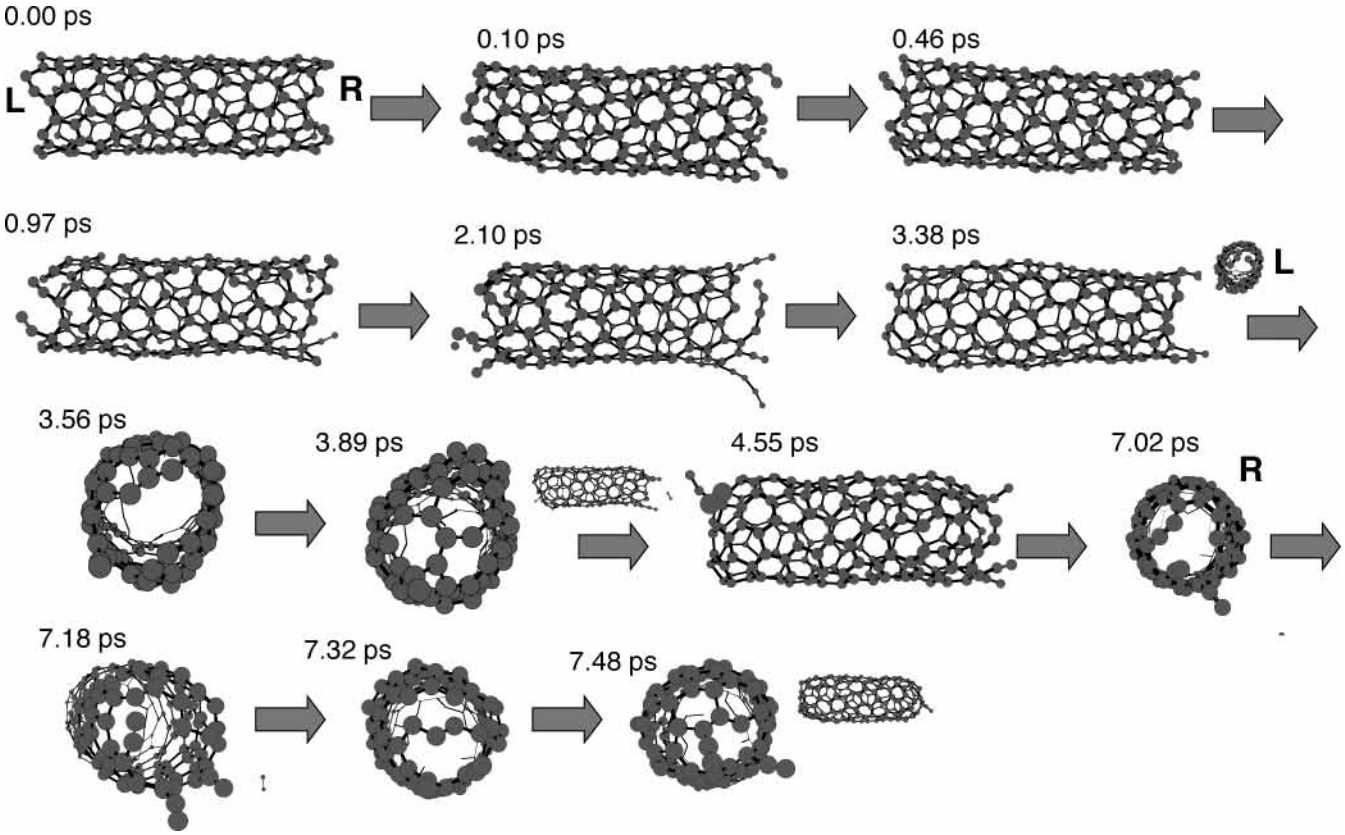

Figure 3. Snapshots of the DFTB trajectory of a 20-Å (7,3) tube at 3000 K.

at the rim is less frequently observed in armchair tube simulations discussed above and is never observed in the trajectories of zigzag nanotubes, confirming the significant difference in the stability of different types of unsaturated openings.[50] At 3.38 ps, both ends are still open. At the R end, only wobbling C_2 units are visible, dangling from an all-hexagon-based rim, while at L three pentagons have formed, two of them connected by a hexagon between them and one single pentagon at the opposite side of the rim (visible at the top of the inserted snapshot). The two connected pentagons reached their positions by sequential 5/6 isomerizations, and together with their attached hexagons, these pentagons achieve significant curvature of the rim inward the opening. Very soon after 0.18 ps, at 3.56 ps, the pentagon-attached hexagon connects with a four-membered ring to its right, and by breaking the four-membered ring, a new 5/6 combination is created. The L side then closes by connecting the top carbon of the new pentagon with the top carbon of a hexagon of another 6/5 configuration at the opposite side at 3.89 ps. Meanwhile, the R side lost a wobbling C_2 unit and features besides hexagons one pentagon in the second layer from the rim and three still attached C_2 units. The embedded pentagon was created earlier by catching the inside atom of a wobbling C_2 unit, leading to the frequently observed structure of a pentagon with single atom on top. The single carbon atom reacted with one of a nearby wobbling C_4 unit, creating the outer hexagon on top of the original pentagon. At 4.55 ps, this outer hexagon becomes transformed into a heptagon by subsequent detachments and reconnections of the outer carbon chain, and this heptagon is able to reach fairly deeply into the opening of the R end, as is visible in the snapshot at 7.02 ps. This side of the tube now has three pentagons and two wobbling C_2 units in addition to a heptagon, with considerable curvature inward. The heptagon isomerizes after a lifetime of about 2.7 ps at 7.18 ps, leading to two hexagons, one being created from the original heptagon and the other one created using one carbon atom as top center in the former gap between the former heptagon and an adjacent pentagon. Subsequent isomerization reactions lead to a carbon bridge in the middle of the opening at 7.32 ps, which is then attacked by a nearby wobbling C_2 unit at 7.48 ps. The opening is finally closed by simultaneously "zipping-up" the remaining rim atoms and the bridge, which became close due to the two previously created bridges. The result is a completely closed 20-Å (7,3) nanotube with 11 pentagons.

Chiral tubes, like armchair tubes, possess cisoid bonds that are very prone to break even under lower temperatures of 2000 K. At higher temperatures, frequently larger wobbling linear carbon chains such as C_4 are formed by a sequence of bond dissociations between rim atoms and the remainder of the tube. This happens particularly often "down the staircase" of chiral tube openings. Structural defects such as this then weaken the π-conjugation stabilization and self-enhance further destruction of the regular hexagon lattice at the openings.

MD of a 20-Å (9,0) Tube at 3000 K. Figure 4 illustrates in 16 snapshot figures the simulation of a 20-Å (9,0) open-ended zigzag tube at 3000 K. In contrast to the armchair and chiral cases, where the first wobbling C_2 unit is created within the first 0.10 ps at the opening rim, it takes this zigzag tube 1.43 ps to develop a wobbling C_2 unit. Our (8,0), (10,0), and other (9,0) zigzag tube trajectories agree with this finding, the fastest time for wobbling C_2 development being 0.181 ps in the 10-Å (10,0) case at 4000 K. Before the development of wobbling C_2 units, large-amplitude motions of the hexagon skeleton, in particular of bonds connecting the outer polyacetylenic rim chain to the tube, can be observed, as shown in the snapshot for 1.28 ps at the L end. At other times, more rarely, bonds of the outer rim chain itself break like in the snapshot for 1.43 ps, which suggests that stand-alone carbon chains are created because the connecting bonds are stretched beyond the 1.8-Å threshold. Most

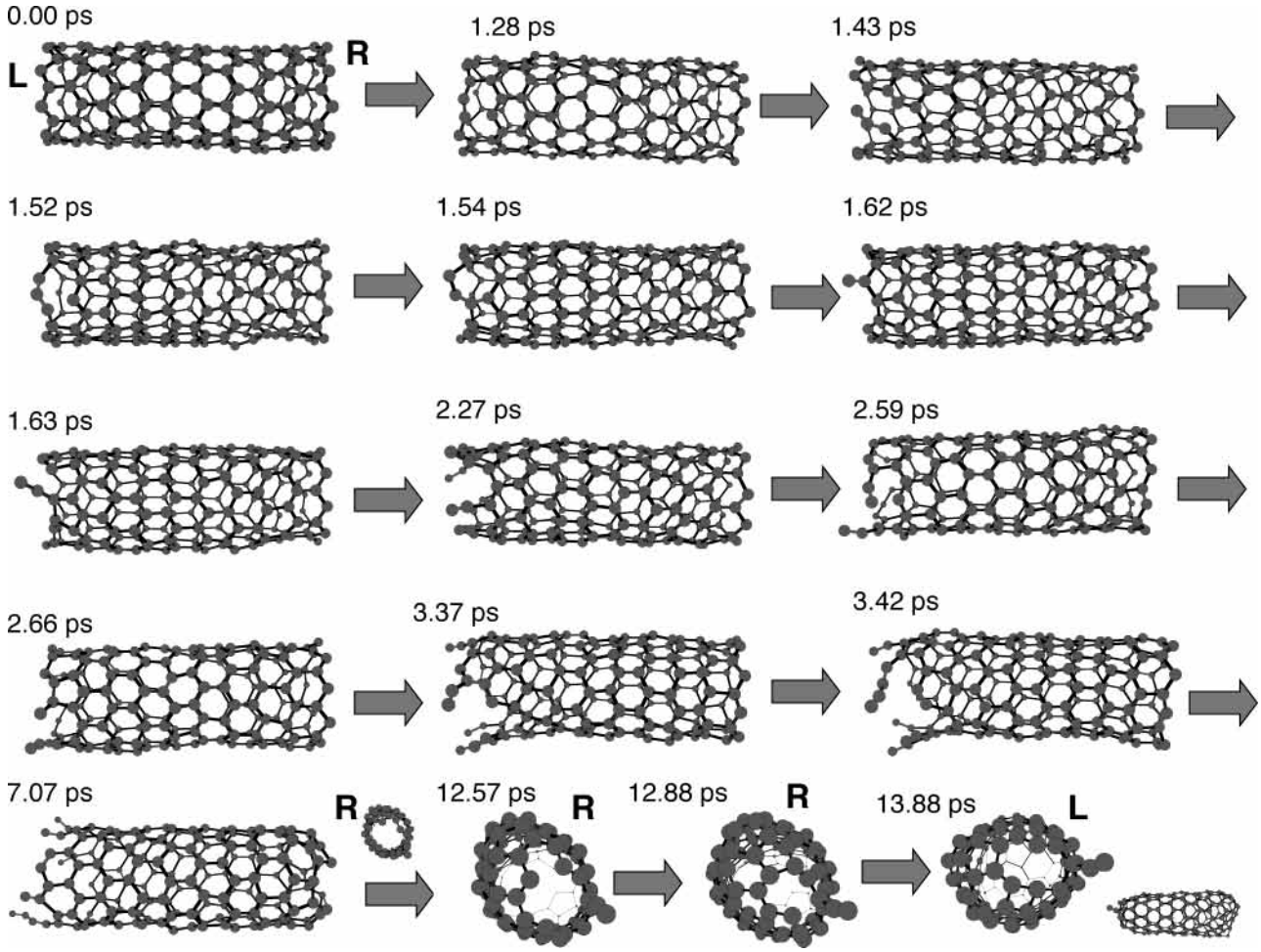

Figure 4. Snapshots of the DFTB trajectory of a 20-Å (9,0) tube at 3000 K.

of the time these bonds snap right back, and the hexagon lattice remains unchanged. The only noticeable event at this early stage in zigzag-tube simulations is Stone−Wales 6/6 to 5/7 rearrangement, which takes place like in the sequence shown here for the L end at 1.52 and 1.54 ps. The created heptagons very often undergo further reconstruction, and in this case, a hexagon with one carbon atom connected to its top is formed at 1.62 ps. This structure is not stable, either, as it falls apart and creates the first, long-lived wobbling C_2 unit at the L end of the tube. This step is important as it allows the introduction of the first destruction of the π-conjugation framework, and at 2.27 ps, a second wobbling C_2 unit appears at the same end, this time by a relative rare deformation involving a three-membered ring formation caused by large amplitude movements of the rim zigzag chain and subsequent bond breaking. The three-membered ring subsequently isomerizes to form a long-lived heptagon. At 2.59 ps, "double wobbling" occurs in the area of the first C_2 unit at L, followed by the formation of a pentagon at 2.65 ps. This pentagon however reisomerizes, and a hexagon is re-created. Meanwhile, no major structural transformations are visible at the R end at all, again demonstrating the self-enhancing effect of defects in one area, which is entirely a π-electronic effect. Stone−Wales-type isomerizations, followed by C_2 unit formation from heptagons, continue to occur at the L end, and at 3.37 ps, four wobbling C_2 units, or two "double wobbling" structures, are visible. In the case of zigzag nanotubes, "double wobbling" creates chiral tubelike "staircases" in the tube sidewalls, and at 3.42 ps, one rim of such a staircase loses one connection and can be seen as a wobbling C_4 unit. At 4.15 ps, the first successful Stone−Wales isomerization at the R end is observed (not shown), and at 7.07 ps, three pentagons have been created, giving this opening a large curvature inward, while no pentagons can be found at the L end. The R ends starts to close at about 12.57 ps with the approach of two hexagons, each of them connected to a pentagon, and a five-membered cyclic gap between them. The new pentagon is formed at 12.59 ps (not shown), and its formation forces the remaining opening to shrink. At 12.88 ps, a pentagon and a four-membered ring, separated by a gap, come sufficiently close to each other to become permanently connected, and the R opening is closed with an octagon as largest macrocycle remaining. The L end closes rather fast after this, having undergone similar isomerizations, and the entire tube is closed at 13.88 ps, with 10 pentagons formed at its caps.

Zigzag tubes are structurally and energetically very different from armchair tubes; they do not possess the easily breakable cisoid bonds of armchair or chiral tubes, and it takes generally very long even at high temperatures for the tubes to form wobbling linear chain defects. Rather, at the initial stage, Stone−Wales 6/6 to 5/7 defects occur increasingly frequently with increasing temperature, allowing the formation of wobbling C_2 units from heptagons, thereby initiating other self-enhanced defects. Once a defect is formed, the zigzag tubes close themselves similarly but somewhat slower than armchair and chiral tubes.

Common Features of DFTB Dynamics. Despite some differences in different types of nanotube trajectories, it is necessary to point out again critical key dynamic events during the transformation from nanotube to closed-cage structures: Mini-

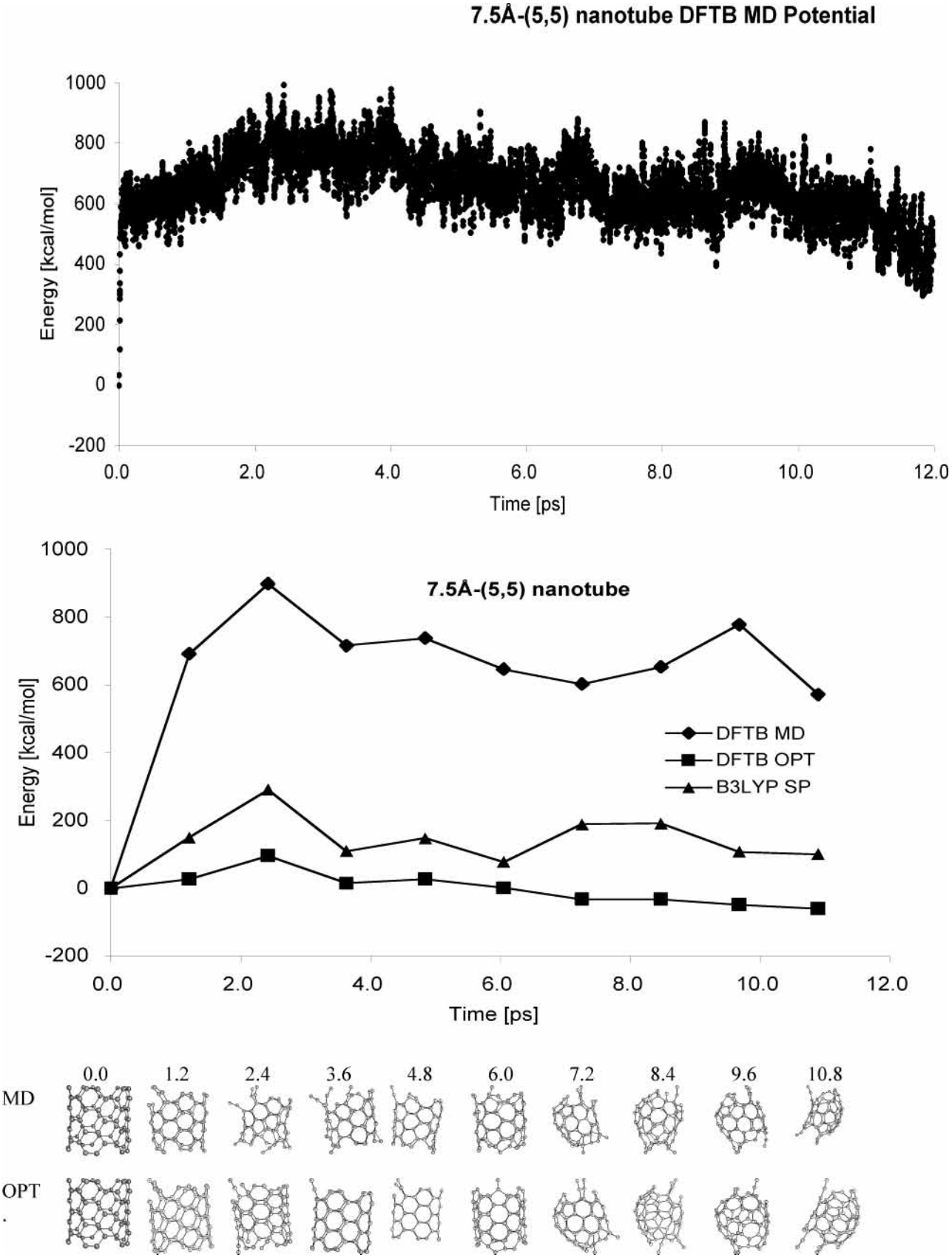

Figure 5. Top: The potential-energy profile of the 7.5-Å (5,5) nanotube DFTB trajectory at 3000 K. Middle and bottom: the DFTB potential energies (◇) and structures (MD) at 10 snapshot points during the 7.5-Å (5,5) tube trajectory at 3000 K, the energies (□) of the structures (OPT) optimized by DFTB from the snapshot points, and the single-point B3LYP/6-31G(d) energy (△) at the DFTB-optimized points. Here, 0 kcal/mol is chosen for the equilibrium open-ended nanotube structure optimized by DFTB to allow comparison to B3LYP energies.

mizing the number of dangling bonds is a well-established driving force for bond formation in carbon clusters and plays a major role in the surprisingly fast closing mechanism of the open-ended model nanotubes of this study.

1. Wobbling C_2 units are stable due to their intrinsic properties. They help to form pentagons, heptagons, and other structural defects to induce some curvature on the rim, which is the important factor of the open-end closure. In general, wobbling linear carbon chains C_n with $1 < n < 5$ appear abundantly as the major structural unit besides hexagons, pentagons, and heptagons in high-temperature molecular dynamics of molecular carbon clusters, n increasing with temperature. Chiral tubes are most apt to long-chain formation, followed by armchair, and zigzag as least likely.

2. Defects at the rims never extend beyond two hexagon layers from the rim, even at 4000 K if the tube is not destroyed completely, or at longer simulation times, as preliminary calculations on a (10,0) tube for 50 ps revealed. This means that there is a distinct limit as to how much a tube opening can bend inward, and this limit is independent of the tube length. Once the tube diameter becomes too large, the tube can no longer close by itself. The threshold diameter size can be estimated from our negative simulations for the (10,0) tube to be about 7.7 Å or possibly somewhat larger.

3. A 5/7 fused 10-membered ring system is more flexible, and the bond between these two rings is weak, which helps to create a larger ten-membered ring resembling a carbon bridge in the opening, giving a chance for attack of C_2 unit and other defects from the opposite side of the openings.

4. [2+4] and larger cycloaddition "zipper"-type reactions occur in the final stage of end close when the opening size has been reduced to an approximately twelve-membered ring. Closing occurs very rapidly, once a critical diameter size has been reached by structural deformations of the rim.

C. B3LYP Calculations of Selected Structures from DFTB/MD Trajectories. The top figure of Figure 5 shows the changes of potential energy during the simulation of a 7.5-Å (5,5) nanotube DFTB trajectory at 3000 K. Starting from 0 kcal/mol at the equilibrium nanotube structure, one can see that the trajectory quickly climbs up a steep hill of potential energy reflecting 3000 K constant temperature, and propagates with the average potential energy of around 400−500 kcal/mol with a fluctuation of ±100 kcal/mol, sometimes even larger. To gain insight into the structures sampled by the trajectory, we took 10 snapshots of the trajectory at 1.21-ps intervals, as shown at the bottom of Figure 3. All these 10 structures were then optimized by DFTB, and single-point energy calculations are performed by B3LYP/6-31G(d). DFTB-optimized energies and B3LYP/6-31G(d) energies are shown in the middle part of Figure 5. The comparison of the DFTB MD structures and DFTB optimized at the bottom of Figure 5 indicates that, while the MD structure have many rings with stretched or compressed bond distances and distorted bond angles, the optimized structures have mostly regular rings with "normal" bond distances and angles. These optimized structures are local minima on potential-energy surfaces and suggest existence of a large number of local minima of different bonding patterns on the nanotube-to-fullerene pathway. The energies of the DFTB-optimized structures are in the range of −59.1 to 96.5 kcal/mol, indicating that these local minima are not much different in energy. We see in Figure 5 that the DFTB-optimized energy climbs up about 100 kcal/mol at the early stage and then declines slowly and continuously as the time progresses, as if seeking for a thermodynamically more stable structure. Of course, caution has to be taken not to over-interpret the result of a single trajectory. The comparison of the DFTB-optimized energies and B3LYP/6-31G(d) single-point energies at DFTB-optimized geometries in the middle of Figure 3 indicates that the two energy profiles are qualitatively parallel, suggesting that DFTB potential surface approximately parallels the B3LYP surface during the dynamics. The average difference in relative energies between the two methods of about 100 kcal/mol can be attributed to the different energetics for the (5,5) tube reference structure.

TABLE 3: DFTB and UB3LYP/3-21G(d) Dissociation Energies (ΔE) of Various Bonds in 7.5-Å (5,5) and (9,0) Tubes

type	bond[a]	DFTB ΔE (kcal/mol)	UB3LYP/3-21G(d) ΔE (kcal/mol)
(5,5)	A	49.0	60.6
	B	24.8	52.8
	C	52.6	114.1
(9,0)	D	38.5	

[a] Bond labels are shown in the structures below.

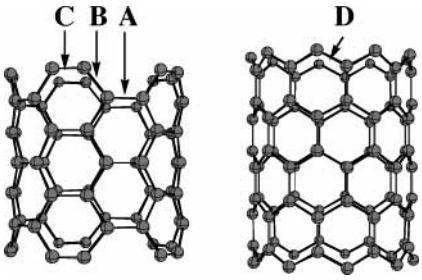

D. Strengths of Rim CC Bonds in Open-Ended Nanotubes. In this section, we make a brief study on what bond is energetically easiest to break in the open-end 7.5-Å (5,5) and (9,0) nanotubes. Table 3 shows the calculated bond dissociation energies for various CC bonds on the open end of the nanotubes. The broken-bond structures (as well as the regular open-end nanotube structures) were optimized both with the DFTB and the spin-unrestricted B3LYP/3-21G(d) method by freezing the length of the broken bond at 2.0 Å. This situation corresponds to an electronic structure with biradical character, and while DFTB does not discriminate between open-shell singlet and triplet, it is necessary to use spin-unrestricted B3LYP to describe the open-shell singlet correctly. Their energies relative to the energy of the fully optimized open-end structures were taken as the bond energies, ΔE. For the armchair-type (5,5) nanotube, the cisoid bond (B) is found to be the weakest bond. This thermodynamic preference is reflected in the results of DFTB dynamics for armchair-type nanotubes at high temperature (1000−4000K) range reported in section B, where cisoid bonds are almost always preferentially broken to form "dangling C_2" units. For the zigzag-type (9,0) nanotubes, there is only one kind of bond (D) at the open end, and Table 2 shows that this bond is stronger that the cisoid bond in the armchair (5,5) nanotubes. This is also reflected in the high temperature DFTB dynamics of zigzag-type nanotubes, where the open end was found to be less easily broken than in armchair-type nanotubes.

E. Trajectories on the REBO Potential. In the present section, we show results of two trajectories on armchair and chiral open-ended tubes at 3000 K, using the original REBO semiempirical force field.[32,33] This potential has been used in previous studies on high-temperature dynamics of carbon clusters by Maruyama et al.,[51−54] before Brenner improved upon it by addressing a flaw concerning the introduction of a spurious force for internuclear distances larger than 1.7 Å.[35] However, the improved version has itself problems with bond-formation processes, which are essential in the closing of carbon nanotubes, and we therefore decided to compare our DFTB calculations with the simulations using the original REBO potential. Both

TABLE 4: Summary of All the REBO Trajectories of Nanotubes of Different Types and Lengths[a]

type (n,m)	length (Å)	no. carbon atoms, n	T (K)	$\langle T \rangle$ (K)	$\langle V \rangle / n$ (kcal/mol)	run time (ps)	no. lost $C_1\|C_2\|C_3$ units	no. final 4/5/6/7-rings
(5,5)	7.5	70	3000	2966	−62.2	19.4	0|0|0	1/0/25/0
(7,3)	7.5	70	3000	2950	−61.1	12.1	0|0|0	0/2/24/0

[a] For details, see Table 2.

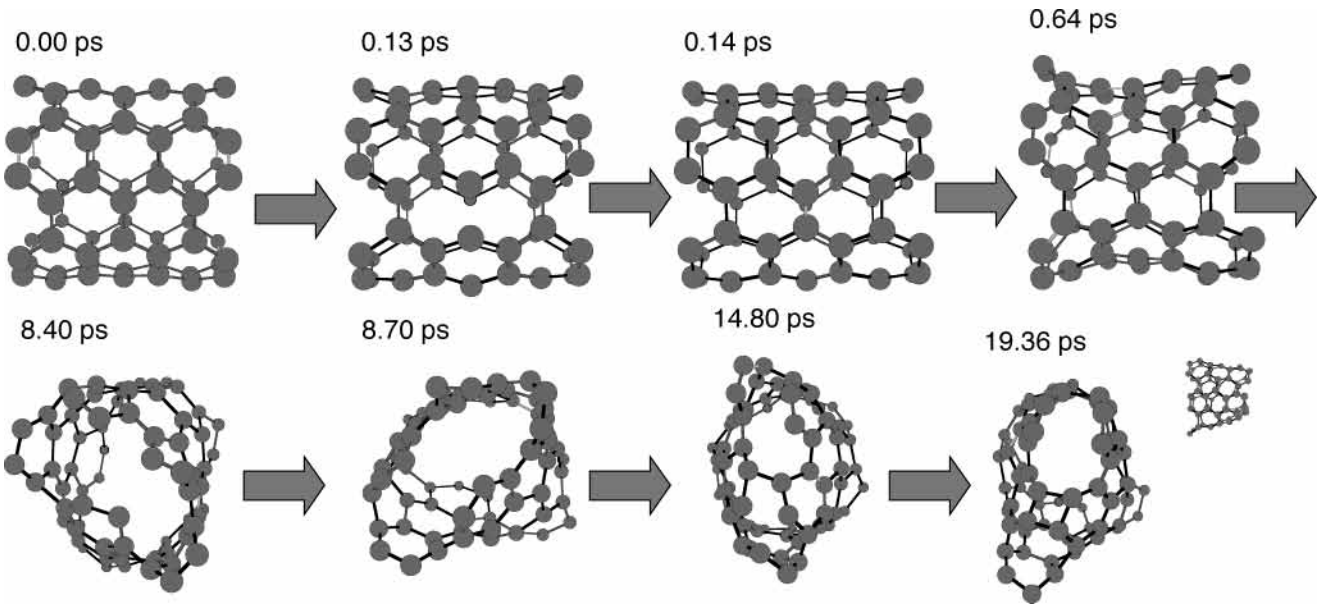

Figure 6. Snapshots of the REBO trajectory of a 7.5-Å (5,5) tube at 3000 K.

armchair and chiral types were found using DFTB to readily close open ends within less than 14 ps, and we therefore chose them as candidates for comparable REBO trajectories. *7.5-Å (5,5) Tube.* Eight snapshots of a 7.5-Å (5,5) nanotube REBO trajectory are shown in Figure 6 up to 19.36 ps. During the entire simulation time, only few bond-breaking and -formation processes are observed. At 0.13 ps, two bonds in the middle of the nanotube break but mend again quickly at 0.14 ps, indicating large amplitude vibrations in the tube interior. Following this event, no permanent bond formation or dissociation processes happen up to 14.80 ps. The snapshots at 8.40 and 8.70 ps show strongly deformed ends of the nanotube, but the hexagon lattice remains intact and neither pentagons, heptagons, nor wobbling C_2 units appear. At 14.80 ps, one new bond forms between two carbons at the end of the nanotube and one more bond forms at the same end at 19.36 ps. However, the end of the nanotube is still open up to 19.36 ps. This simulation shows the difficulty of the REBO force field to break carbon−carbon σ bonds under 3000 K, and hence major restructuring of the tube's honeycomb lattice to accommodate pentagons and greater curvature requires a much longer time.

7.5-Å (7,3) Tube. In Figure 7, 10 snapshots of a 7.5-Å (7,3) nanotube REBO trajectory are presented. At 0.02 ps, several hexagons at end L and end R become vibrationally strongly excited, and their outer bonds become stretched beyond the 1.8-Å threshold. In fact, the broken bonds remain broken for 0.25 ps. Single, isolated carbon atoms are created by this mechanism, which is different from the formation of wobbling C_2 units in the DFTB trajectories. At 0.27 ps, these broken bonds recombine back to intact hexagons at the rims of nanotube. At 0.73 ps, a fused 5/7 ring is formed in a Stone−Wales-type isomerization from two fused hexagons. After about 5.78 ps, we do not find more isomerization reactions of the hexagon lattice, very similar to the above (5,5) nanotube. The fused 5/7 ring back transforms into two fused hexagons via retro-Stone−Wales isomerization.

From the above description of two trajectories of different types of nanotubes, it clearly shows that, in trajectories based on the REBO semiempirical potential function, few bond-formation and -dissociation processes are observed, at least within up to 20 ps. This finding is very different from our previously described trajectories using the DFTB quantum chemical potential method. It is due to intrinsic deficiency of the REBO potential. In REBO potential, the interaction is calculated according to the distance between two adjacent atoms, which obviously cannot properly include nonlocal effects,[32] such as π-conjugational effects. However, π-conjugational effects appear to be the origin for self-enhanced multiple defect formation and are an essential ingredient in DFTB trajectories. REBO does not include such nonlocal changes in energetics and remains indeed "adamant" toward breaking an established σ-bonded carbon network. We note that REBO carbon trajectories at 5000 K are typically discussed in terms of nanoseconds,[54] whereas QM/MD simulations on carbon nanostructures can be described within less than 100 picoseconds.[38,55]

IV. Concluding Remarks

1. Benchmark calculations on some representative C_{28} structures indicated that the DFTB method is very reasonable in reproducing the reference B3LYP/6-31(d) relative energies at a small fraction of computation costs, in agreement with tests by other groups.

2. DFTB trajectories of different types of open-ended nanotubes calculated by the DFTB method are reviewed in detail. Wobbling C_2 units play an important role in the closure of the open ends to give fullerenes. The existing wobbling C_2 units create new pentagons as well as hexagons and heptagons at the edges and thus bring curvature into the structure that

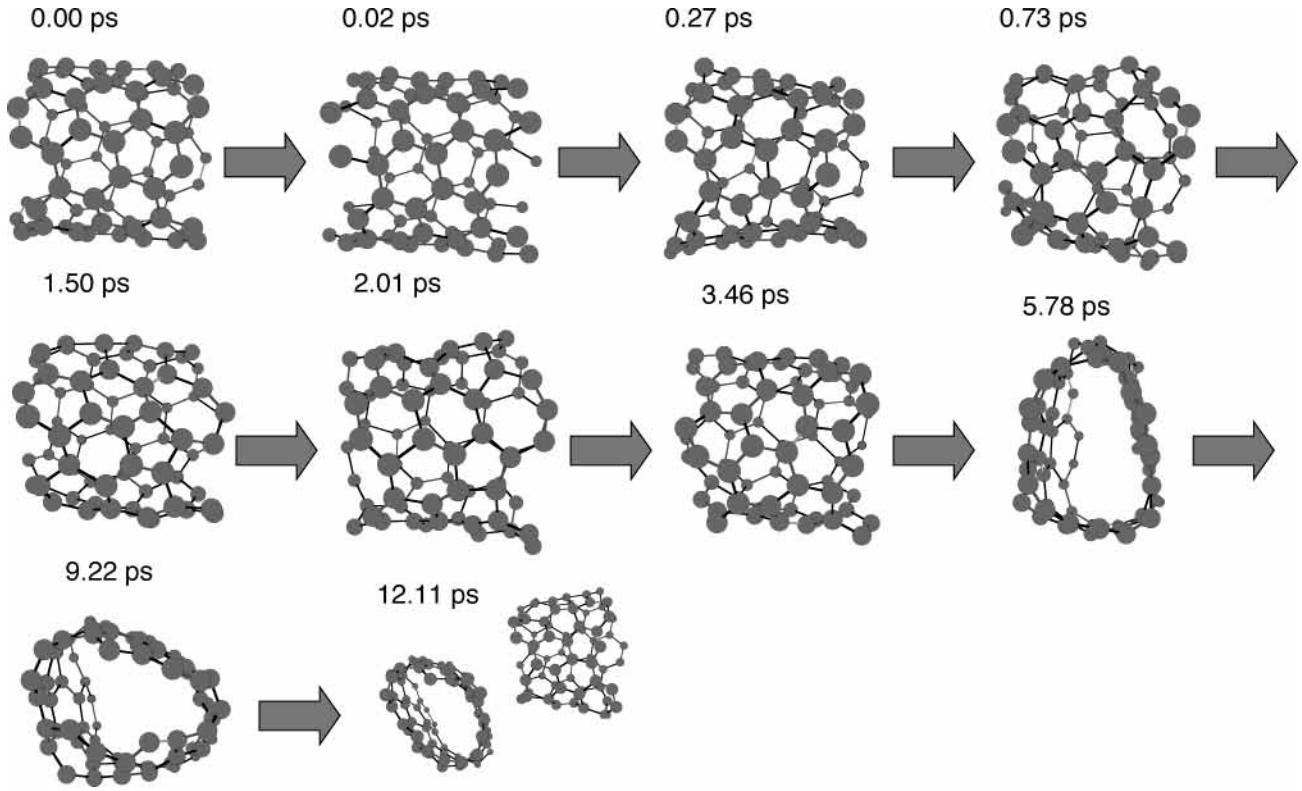

Figure 7. Snapshots of the REBO trajectory of a 7.5-Å (7,3) tube at 3000 K.

finally closes. Once a wobbling C_2 unit is created, π conjugation is interrupted in this area, and more wobbling C_2 units follow in the vicinity of the first. Stone−Wales isomerization takes place often during the nanotube-to-fullerene transformation.

3. From snapshots of these trajectories, structures were optimized at the DFTB level and B3LYP/6-31(d) single-point calculations were performed. The calculated B3LYP potential-energy profiles are nearly parallel to the DFTB potential profiles, suggesting that MD with DFTB is a practical approximation to B3LYP.

4. The initial bond-breaking patterns are studied as well as the associated energy potential surfaces. As observed in the trajectories that wobbling C_2 units are hard to form at the rim of zigzag nanotubes, the energy results for different initial stages of bond breaking processes show that the bond at the rim of zigzag nanotubes is much harder to break compared with that of armchair or chiral nanotubes, which is the reason wobbling C_2 units are rarely found at the initial stages of zigzag nanotubes, while in armchair and chiral nanotubes, wobbling C_2 units form much more often and very quickly.

5. Trajectories using the REBO potential give less-active bond-dissociation and -formation events than those using DFTB, reflecting the lack of π conjugation effects in the REBO method.

Acknowledgment. This work was partially supported by a grant from the Mitsubishi Chemical Corporation and from the Petroleum Research Fund, the American Chemical Society. Acknowledgment is made to the Cherry L. Emerson Center of Emory University for the use of its resources, which is in part supported by a National Science Foundation Grant (CHE-0079627) and an IBM Shared University Research Award. We also thank the National Center for Supercomputing Applications (NCSA) for valuable supercomputer time and one reviewer for insightful and very helpful comments.

References and Notes

(1) Kroto, H. W.; Heath, J. R.; O'Brien, S. C.; Curl, R. F.; Smalley, R. E. *Nature* **1985**, *318*, 162−163.
(2) Krätschmer, W.; Fostiropoulos, K.; Huffman, D. R. *Chem. Phys. Lett.* **1990**, *170*, 167−170.
(3) Kroto, H. W.; Allaf, A. W.; Balm, S. P. *Chem. Rev.* **1991**, *91*, 1213−1235.
(4) Gerhardt, P.; Löffler, S.; Homann, K.-H. *Chem. Phys. Lett.* **1987**, *137*, 306−310.
(5) Gerhardt, P.; Löffler, S.; Homann, K.-H. *Proc. Combust. Inst.* **1989**, *22*, 395−401.
(6) Howard, J. B.; McKinnon, J. T.; Makarovsky, Y.; Lafleur, A. L.; Johnson, M. E. *Nature* **1991**, *352*, 139−141.
(7) Howard, J. B.; McKinnon, J. T.; Johnson, M. E.; Makarovsky, Y.; Lafleur, A. L. *J. Phys. Chem.* **1992**, *96*, 6657−6662.
(8) Howard, J. B.; Lafleur, A. L.; Makarovsky, Y.; Mitra, S.; Pope, C. J.; Yadav, T. K. *Carbon* **1992**, *30*, 1183−1201.
(9) Pope, C. J.; Marr, J. A.; Howard, J. B. *J. Phys. Chem.* **1993**, *97*, 11001−11013.
(10) Kroto, H. W.; McKay, K. *Nature* **1988**, *331*, 328−331.
(11) Kroto, H. W. *Science* **1988**, *242*, 1139−1145.
(12) Kroto, H. W. *Carbon* **1992**, *30*, 1139−1141.
(13) Curl, R. F.; Smalley, R. E. *Sci. Am.* **1991**, *265*, 54−63.
(14) Haufler, R. E.; Chai, Y.; Chibante, L. P. F.; Conceicao, J.; Jin, C.; Wang, L.-S.; Maruyama, S.; Smalley, R. E. *Mater. Res. Soc. Symp. Proc.* **1991**, *206*, 627−637.
(15) Smalley, R. E. *Acc. Chem. Res.* **1992**, *25*, 98−105.
(16) Heath, J. R. *ACS Symp. Ser.* **1991**, *481*, 1−23.
(17) Wakabayashi, T.; Shiromaru, H.; Kikuchi, K.; Achiba, Y. *Chem. Phys. Lett.* **1993**, *201*, 470−474.
(18) van Helden, G.; Gotts, N. G.; Bowers, M. T. *Nature* **1993**, *363*, 60−63.
(19) Hunter, J.; Fye, J.; Jarrold, M. F. *Science* **1993**, *260*, 784−786.
(20) Lagow, R. J.; et al. *Science* **1995**, *267*, 362−367.
(21) Goroff, N. S. *Acc. Chem. Res.* **1996**, *29*, 77−83.
(22) Lozovik, Y. E.; Popov, A. M. *Phys.−Usp.* **1997**, *40*, 717−737.
(23) Strout, D. L.; Scuseria, G. E. *J. Phys. Chem.* **1996**, *100*, 6492−6498.
(24) Bates, K. R.; Scuseria, G. E. *J. Phys. Chem. A* **1997**, *101*, 3038−3042.
(25) Jones, R. O. *J. Chem. Phys.* **1999**, *110*, 5189−5200.
(26) Portmann, S.; Galbraith, J. M.; Schaefer, H. F.; Scuseria, G. E.; Lüthi, H. P. *Chem. Phys. Lett.* **1999**, *301*, 98−104.
(27) Dewar, M. J. S.; Zoebisch, E. G.; Healy, E. F.; Stewart, J. J. P. *J. Am. Chem. Soc.* **1985**, *107*, 3902−3909.

(28) Mishra, R. K.; Lin, Y.-T.; Lee, S.-L. *J. Chem. Phys.* **2000**, *112*, 6355−6364.
(29) Schweigert, V. A.; Alexandrov, A. L.; Morokov, Y. N.; Bedanov, V. M. *Chem. Phys. Lett.* **1995**, *235*, 221−229.
(30) Tersoff, J. *Phys. Rev. B* **1988**, *37*, 6991.
(31) Tersoff, J. *Phys. Rev. B* **1989**, *39*, 5566.
(32) Brenner, D. W. *Phys. Rev. B* **1990**, *42*, 9458−9471.
(33) Brenner, D. W. *Phys. Rev. B* **1992**, *46*, 1948.
(34) Stuart, S. J.; Tutein, A. B.; Harrison, J. A. *J. Chem. Phys.* **2000**, *112*, 6472−6486.
(35) Shenderova, O. A.; Brenner, D. W.; Omeltchenko, A.; Su, X.; Yang, L. H. *Phys. Rev. B* **2000**, *61*, 3877−3888.
(36) Porezag, D.; Frauenheim, T.; Köhler, T.; Seifert, G.; Kaschner, R. *Phys. Rev. B* **1995**, *51*, 12947−12957.
(37) Seifert, G.; Porezag, D.; Frauenheim, T. *Int. J. Quantum Chem.* **1996**, *58*, 185−192.
(38) Irle, S.; Zheng, G.; Elstner, M.; Morokuma, K. *Nano Lett.* **2003**, *3*, 465−470.
(39) Elstner, M.; Porezag, D.; Jungnickel, G.; Elsner, J.; Haugk, M.; Frauenheim, T.; Suhai, S.; Seifert, G. *Phys. Rev. B* **1998**, *58*, 7260−7268.
(40) Frisch, M. J.; Trucks, G. W.; Schlegel, H. B.; Scuseria, G. E.; Robb, M. A.; Cheeseman, J. R.; Montgomery, J. A., Jr.; Vreven, T.; Kudin, K. N.; Burant, J. C.; Iyengar, S. S.; Millam, J. M.; Tomasi, J.; Barone, V.; Mennucci, B.; Cossi, M.; Scalmani, G.; Rega, N.; Petersson, G. A.; Ehara, M.; Toyota, K.; Hada, M.; Fukuda, R.; Hasegawa, J.; Ishida, M.; Nakajima, T.; Kitao, O.; Nakai, H.; Honda, Y.; Nakatsuji, H.; Li, X.; Knox, J. E.; Hratchian, H. P.; Cross, J. B.; Adamo, C.; Jaramillo, J. J.; Cammi, R.; Pomelli, C.; Gomperts, R.; Stratmann, R. E.; Ochterski, J.; Ayala, P. Y.; Morokuma, K.; Salvador, P.; Dannenberg, J. J.; Zakrzewski, V. G.; Dapprich, S.; Daniels, A. D.; Strain, M. C.; Farkas, O.; Malick, D. K.; Rabuck, A. D.; Raghavachari, K.; Foresman, J. B.; Ortiz, J. V.; Cui, Q.; Baboul, A. G.; Clifford, S.; Cioslowski, J.; Stefanov, B. B.; Liu, G.; Liashenko, A.; Piskorz, P.; Komaromi, I.; Martin, R. L.; Fox, D. J.; Keith, T.; Al-Laham, M. A.; Peng, C. Y.; Nanayakkara, A.; Challacombe, M.; Gill, P. M. W.; Johnson, B.; Chen, W.; Wong, M. W.; Gonzalez, C.; Pople, J. A. *Gaussian 01*, Development Version, revision B.02+; Gaussian, Inc.: Pittsburgh, PA, 2002.
(41) Bode, B. M.; Gordon, M. S. *J. Mol. Graphics Modell.* **1998**, *16*, 133−138.
(42) Fowler, P. W.; Heine, T.; Mitchell, D.; Orlandi, G.; Schmidt, R.; Seifert, G.; Zerbetto, F. *J. Phys. Chem.* **1996**, *100*, 6984−6991.
(43) Fowler, P. W.; Heine, T.; Mitchell, D.; Orlandi, G.; Schmidt, R.; Seifert, G.; Zerbetto, F. *J. Chem. Soc., Faraday Trans.* **1996**, *92*, 2203−2210.
(44) Fowler, P. W.; Heine, T.; Rogers, K. M.; Sandall, J. P. B.; Seifert, G.; Zerbetto, F. *Chem. Phys. Lett.* **1999**, *300*, 369−378.
(45) Jungnickel, G.; Porezag, D.; Köhler, T.; Frauenheim, T.; Pedersen, M. R. In *Fullerenes and Fullerene Nanostructures*; Kuzmany, H., Ed.; World Scientific: Singapore: Kirchberg, Austria, 1996; pp 305−318.
(46) Domene, M. C.; Fowler, P. W.; Mitchell, D.; Seifert, G.; Zerbetto, F. *J. Phys. Chem. A* **1997**, *101*, 8339−8344.
(47) Stewart, J. J. P. *J. Comput. Chem.* **1989**, *10*, 209−220.
(48) Chen, Z.; Thiel, W. *Chem. Phys. Lett.* **2003**, *367*, 15−25.
(49) Zhou, H.; Tajkhorshid, E.; Frauenheim, T.; Suhai, S.; Elstner, M. *Chem. Phys.* **2002**, *277*, 91−103.
(50) Oh, D.-H.; Lee, Y. H. *Phys. Rev. B* **1998**, *58*, 7407−7411.
(51) Maruyama, S.; Yamaguchi, Y. *Trans. JSME* **1997**, *63−611B*, 2405−2412.
(52) Maruyama, S.; Yamaguchi, Y. *Chem. Phys. Lett.* **1998**, *286*, 343−349.
(53) Yamaguchi, Y.; Maruyama, S. *Trans. JSME* **1997**, *63−611B*, 2298−2404.
(54) Yamaguchi, Y.; Maruyama, S. *Chem. Phys. Lett.* **1998**, *286*, 336−342.
(55) Irle, S.; Zheng, G.; Elstner, M.; Morokuma, K. *Nano Lett.* **2003**, *3*, 1657−1664.